Optik 125 (2014) 1962–1966

Contents lists available at ScienceDirect

Optik

journal homepage: www.elsevier.de/ijleo

Nanoscale synthesis and optical features of nickel nanoparticles

M. Hemalatha[a,*], N. Suriyanarayanan[b], S. Prabahar[c]

[a] Department of Physics, Dhanalakshmi Srinivasan College of Engineering, Coimbatore 641105, India
[b] Department of Physics, Government College of Technology, Coimbatore 641018, India
[c] Department of Physics, Tamilnadu College of Engineering, Coimbatore 641659, India

ARTICLE INFO

Article history:
Received 7 May 2013
Accepted 28 September 2013

Keywords:
Synthesis
Nanoparticles
Nickel
Chemical reduction method

ABSTRACT

Nickel nanoparticles have been synthesized by chemical reduction method. By the analysis of X-ray diffraction, the resultant particles are characterized and found to be pure crystalline nickel with a face-centered cubic (FCC) structure. The morphology and size of the nanoparticles are studied by scanning electron microscopy (SEM) and micrographs reveal that the nanoparticles are mostly spherical. The compositional analysis has been carried out by using EDAX. The quantum size confinement of the crystallites is evident from the blue-shift of the absorption edge in the UV–vis absorption spectrum.

© 2013 Elsevier GmbH. All rights reserved.

1. Introduction

Increased attention has been recently paid to the study of metal nanoparticles exhibiting novel optical, electronic, magnetic and chemical properties that are ascribed to the extremely small dimensions and special surface nature [1–5]. Metallic nickel can exist in two crystalline forms with FCC and HCP structure. Almost all common nickel powders are ferromagnetic substances with FCC crystal structure. Among the various kinds of metal nanoparticles, the preparation of some metal nanoparticles such as nickel, copper, and iron, is relatively difficult because they undergo easy oxidation affecting their catalytic performance [6]. Until now, only a few works on the preparation of nickel nanoparticles have been reported and they usually are performed in organic media to avoid the formation of nickel oxide or hydroxide [7]. It is reported that nickel powder has been produced for multilayer ceramic capacitors in cellular phones and mobile computers [11]. Many techniques have been used to prepare the metal nanoparticles, such as chemical reduction [8–12], electrochemical reduction [13], photochemical reduction [14], sonochemical method [15], polyol process [16], heat evaporation [17], and micro emulsion technique [18]. The physical methods always need a high temperature [19], vacuum and expensive equipments, but the conditions that are required by chemical methods are not so critical. The chemical reduction method is one of the commonest methods to synthesize colloidal metal particles because of its convenient operation, easy controlling and simple equipment requirements. Among metal nanoparticles of nickel, iron and cobalt, nickel is the most stable particle. However, few literatures on the preparation of metal nanoparticles have been reported. In present work, we have prepared nickel nanoparticles using hydrazine reduction method and its structural morphologies and optical features of the prepared samples are studied. In the absence of soluble polymer or other extra protective agent, nickel nanoparticles are synthesized in ethylene glycol with hydrazine hydrate as protective agent as well as reducing agent.

2. Experimental

Ethylene glycol was supplied by Merck, India. Nickel chloride hexahydrate and hydrazine hydrate were obtained from Mumbai. Sodium hydroxide (NaOH) pellets were obtained from Loba Chemie. The deionized water was used throughout the experiment. Nickel sample was prepared by the methods reported earlier [9,20], using nickel chloride hexahydrate as a precursor and hydrazine hydrate as reducing agent.

For sample-A preparation, appropriate amount of $NiCl_2$ is dissolved in10 ml ethylene glycol. Then 5 ml hydrazine hydrate is added to above solution. NaOH, which acts as a catalyst of 10–92 μ/ml, are added in sequence and stirred well. The complete solution is kept in water bath for 1 h at 90 °C. During heating bluish green color precipitate slowly changed in to black color, indicating the formation of nickel nanoparticles. These nanoparticles are cooled and collected, washed several times by ethanol and dried in the room temperature (Sample-A). For sample-B preparation; appropriate amount of $NiCl_2$ is dissolved in10 ml ethylene glycol.

* Corresponding author. Tel.: +91 9486114497; fax: +91 4286 245577.
E-mail address: mhlhemu@gmail.com (M. Hemalatha).

0030-4026/$ – see front matter © 2013 Elsevier GmbH. All rights reserved.
http://dx.doi.org/10.1016/j.ijleo.2013.09.069

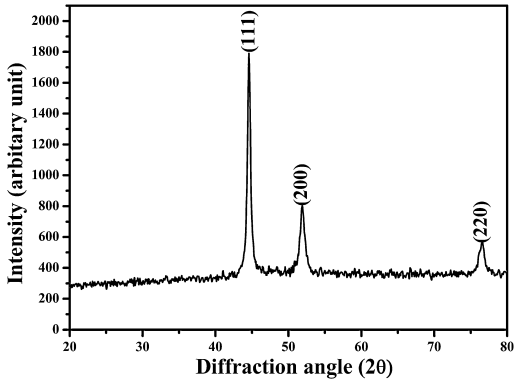


Fig. 1. XRD of nickel nanoparticles (sample-A).

Then 10 ml hydrazine hydrate is added to above solution. NaOH, which acts as a catalyst of 10–92 μ/ml, were added in sequence and stirred well. The complete solution is kept in water bath for 1 hr at 90 °C. During heating bluish green color precipitate slowly changed in to black color, indicating the formation of Nickel nanoparticles. These nanoparticles are cooled and collected, washed several times by ethanol and dried in the room temperature (sample-B). It is seen that N_2 gas is continuously bubbled up in the reaction. It automatically creates N2 atmosphere during the reaction. Hence, no extra N_2 gas is required for the synthesis of nickel nanoparticles. The structural aspects of the Nickel powder are analyzed using X-ray diffractometer with filtered CuKα radiation (λ = 1.5418 Å). The optical absorption measurements are recorded in the wavelength range of 200–800 nm using JASCO V-570 Spectrophotometer.

3. Results and discussion

3.1. Structural analysis

Figs. 1 and 2 show the X-ray diffraction pattern of Ni nanoparticles (sample-A and -B). From Fig. 1 three characteristic peaks for nickel [2θ = 44.56°, 51.85°, 76.00°] corresponding to Miller indices (1 1 1), (2 0 0), (2 2 0) are observed. This revealed that the resultant particles are pure face-centered cubic (FCC) nickel. In Fig. 1, the intensity ratio of the peaks [1 1 1]:[2 0 0]:[2 2 0] are calculated to be [100,26,13] which exactly coinciding with the JCPDS [no: 040850] values. This confirms the presence of Nickel particles in the sample. Fig. 2 shows a typical XRD pattern of the nickel sample-B. From Fig. 2 three characteristic peaks for nickel [2θ = 44.41°, 51.72°, 76.30°] corresponding to Miller indices (1 1 1), (2 0 0), (2 2 0) are observed. This revealed that the resultant particles are pure face-centered cubic (FCC) nickel. No obvious peaks of nickel oxides and

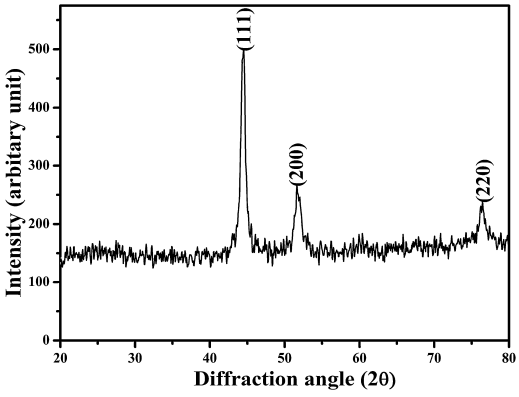


Fig. 2. XRD of nickel nanoparticles (sample-B).

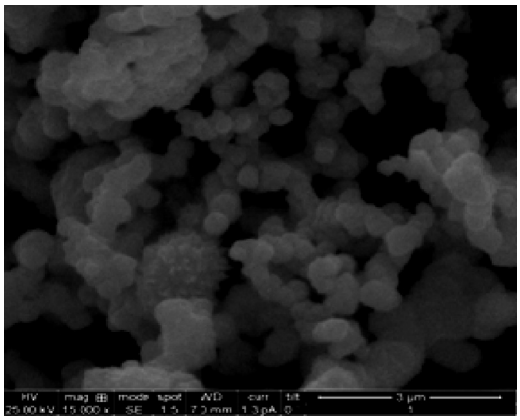


Fig. 3. SEM images of Ni nanoparticles (sample-A).

hydroxides are detected, possibly it is attributed to the observed phenomenon that nitrogen gas is produced and bubbled up continuously during the reaction. It could be suggested that the above said gas produced might auto create an inert atmosphere; hence the input of extra nitrogen gas was not necessary for the synthesis of nickel nanoparticles [9]. In Fig. 2 the intensity ratio of the peaks [1 1 1]:[2 0 0]:[2 2 0] are calculated to be [100,25,14] which exactly coinciding with the JCPDS [no: 040850] values. This confirms the presence of Nickel particles in the sample and it is in good agreement with the earlier reports [18,21,22]. The XRD pattern shows the presence of Ni with almost no peaks corresponding to Ni-oxide. This also indicates that the Ni nanoparticles prepared in this work have high purity.

From the full width at half maximum, the average grain size for the samples can be calculated. For the (1 1 1), (2 0 0), (2 2 0) diffraction peak, according to the Scherrer formula:

$$d = \frac{K\lambda}{\beta}\cos\theta \quad (1)$$

where d is the grain size; $K = 0.89$ is the Scherrer constant related to the shape and index ($h\,k\,l$) of the crystal; λ is the wavelength of the X-rays; θ is the diffraction angle; and B is the corrected full width at half maximum (in radians). This calculation results in an average grain size of 23.64 and18.62 nm for sample-A and sample-B respectively, which is consistent with the average particle diameter obtained from SEM images of Figs. 3 and 4.

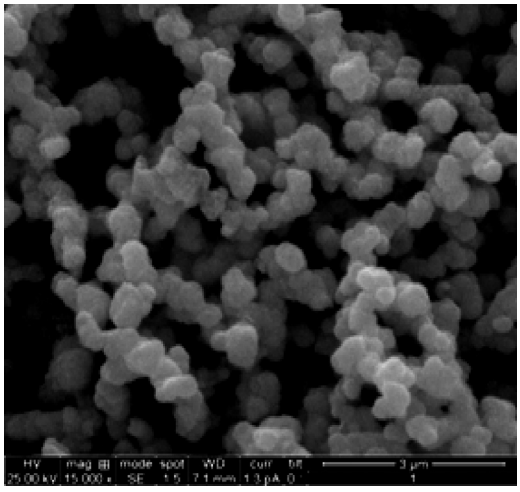


Fig. 4. SEM images of Ni nanoparticles (sample-B).

Table 1
Comparison of XRD data for nickel nanoparticles with the JCPDS card (65-2435).

Different concentration	Planes (*h k l*)	2θ values (°)		d-Spacing values, *d* (Å)		Lattice constant, *a* (Å)	FWHM (β)
		JCPDS	Experimental	JCPDS	Experimental		
Sample-A	1 1 1	44.49	44.56	2.034	2.031	3.5177	0.4
	2 0 0	51.84	51.85	1.762	1.761	3.5219	1
	2 2 0	76.37	76.00	1.245	1.244	3.5185	1
Sample-B	1 1 1	44.49	44.41	2.034	2.038	3.5299	0.64
	2 0 0	51.84	51.72	1.762	1.765	3.5300	1
	2 2 0	76.37	76.30	1.245	1.246	3.5242	1

Table 2
The Structural parameters of Nickel nanoparticles.

Different concentration	2θ values (°)	Grain size, *D* (nm)	Strain (ε)	Dislocation density ($\times 10^{15}$ lines/m^2)
Sample-A	44.56	37.08	0.0925	0.73
	51.85	15.24	0.2247	4.4
	76.00	17.41	0.1970	3.4
Sample-B	44.41	23.17	0.148	1.8
	51.72	15.26	0.224	4.4
	76.30	17.45	0.196	3.4

Table 3
Preferential orientation factor of nickel nanoparticles.

Different concentration	Planes (*h k l*)	Orientation factor (*f*)
Sample-A	1 1 1	1.29
	2 0 0	0.34
	2 2 0	0.21
Sample-B	1 1 1	1.05
	2 0 0	0.36
	2 2 0	0.28

According to the theory of X-ray diffraction, the relation between the interplanar spacing's $d_{h\,k\,l}$ and the diffraction angle can be expressed as:

$$2d_{h\ k\ l}\cos\theta \tag{2}$$

For the FCC structure, the lattice parameter a of a given plane with Miller indices (*h k l*) can be derived using the equation:

$$D_{h\ k\ l} = \frac{a}{\sqrt{h^2 + k^2 + l^2}} \tag{3}$$

The results of the calculations for the (1 1 1), (2 0 0) and (2 2 0) planes for the various samples are presented in Table 1 along with the corrected full width at half maximum (FWHM), the grain size d and the lattice parameter a of the Ni nanoparticles. The lattice parameters for these Ni nanoparticles are always larger than the equilibrium values of the perfect single crystal Ni lattice (a_0 = 0.3523 nm). Lattice parameter decrease with decrease in grain size for sample-A. With decreasing grain size, lattice parameter increase for sample-B. This is abnormal for it was anticipated that the lattice constant of a nanoparticle would be smaller than bulk value according to the point of view of Yu and co-workers [23]. This lattice expansion is the result of the interfacial energy and mutual surface tension attraction of Ni nanoparticles (Tables 2–4).

The intensity of the peak (1 1 1) increases significantly faster than other peaks [(2 0 0) and (2 2 0)] indicating a relatively preferred structural orientation in the (1 1 1) plane. A method that evaluates the magnitude of the preferred orientation factor '*f*' for a given plane (peak) relative to other planes (peaks) in a material is employed. According to this method the preferred orientation factor f (1 1 1) of the (1 1 1) plane for the nickel nano particles has been calculated by evaluating the fraction of (1 1 1) plane intensity over the sum of intensities of all peaks within a given measuring 2θ range [20–80°]. Similarly, the orientation factor of all other peaks has been evaluated for the sample-B. The orientation factor for sample-A have been calculated from Fig. 1and found to be *f*(1 1 1) = 1.05, *f*(2 0 0) = 0.366 and *f*(2 2 0) = 0.28. The orientation factor for sample-B have been calculated from Fig. 2 and found to be *f*(1 1 1) = 1.22, *f*(2 0 0) = 0.33 and *f*(2 2 0) = 0.25 since *f*(0 0 2) is greater compared to other orientation factors in two samples, it can be concluded that nickel nanoparticles have the preferential orientation along (1 1 1) plane. The enhancement of (1 1 1) plane and improved crystalline is remarkable irrespective of the chemical reduction. In this work, at a low hydrazine concentration formation of larger particles could be attributed to the fact that the reduction rate of nickel chloride is slow and only few nuclei are formed. But, when the hydrazine concentration is increased, nickel chloride is reduced faster and due to that, all nickel ions are reduced to atoms before the formation of nuclei. So, the increase of hydrazine concentration leads to the formation of smaller nickel nanoparticles.

Table 4
EDAX analysis of nickel nanoparticles.

Different concentration	Element weight % (Ni)	Atomic % (Ni)
Sample-A	98.59	95.01
Sample-B	98.08	93.29

3.2. Surface morphological studies

The particle size, shape and morphology are identified using SEM micrographs. SEM images of the obtained nickel nanoparticles for the sample-A and sample-B are shown in Figs. 3 and 4. The SEM images show a typical morphology of nickel nanoparticles. The shape of the particles is nearly spherical with homogeneous size distribution. Nickel nanoparticles are in the range of 23.64 and 18.62 nm. The crystallite size calculated from SEM analysis is quite agreement with that of crystallite size calculated from XRD analysis. In the reducing condition, the magnetic nanoparticles are free, so that the motion or rotation of the nanoparticle itself is easy. Because the anisotropic nature of the dipolar interaction favors the formation of the magnetic nano chains, the spontaneous self-assembly of the nanoparticles in to unique structures such as nanochains occurs. As we know, the evolution of a solid from liquid involves two fundamental steps, i.e., nucleation and growth. The key factor

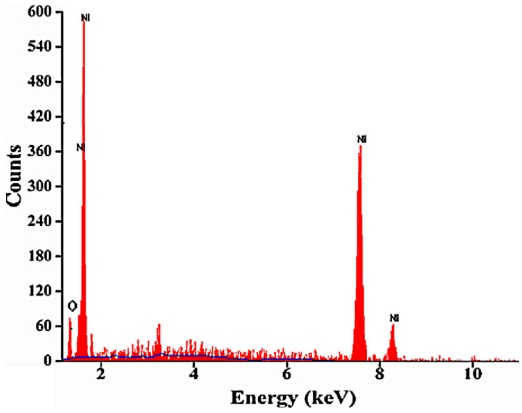


Fig. 5. EDAX spectra of Ni nanoparticles (sample-A).

for the formation of spherical nanoparticles might be due to the difference of chemical environment of the nucleation and growth process.

3.3. EDAX

EDAX analysis verified the composition of the small particles. EDAX analysis on various regions confirmed the presence of pure nickel. This observation correlates with the XRD as well as the optical results. EDAX analysis is used to analyze the ingredients of its composition, indicating that the fabricated nanoparticles contain elements of Ni and O. EDAX analysis result shows that in samples-A and -B the weight percentage of O is 1.41% and 1.92% only, whereas that of Ni is as high as 98.59% and 98.08%. Then, upon the comparison of XRD analysis, it is observed that the fabricated nanoparticles have high percentage of pure nickel, as well as small quantities of oxides. The oxygen detected could be attributed to partial oxidation of the nanoparticles which is due to the presence of some residual solvent or during the handling of the sample (Figs. 5 and 6).

3.4. Optical studies

Fig. 7 is the UV–vis spectrum of the as-synthesized pure nickel nanoparticles. A strong absorption in the UV region is observed at wavelengths about 371 nm for the particle size of 23.64 nm (sample-A). From Fig. 8, the absorption band is observed at 321 nm for the particle size of 18.62 nm (sample-B). Curtis et al. [24] found that nickel bulk absorption presents, a band centered near 230 nm. Galo Cardenas et al. have reported that nickel particles of size

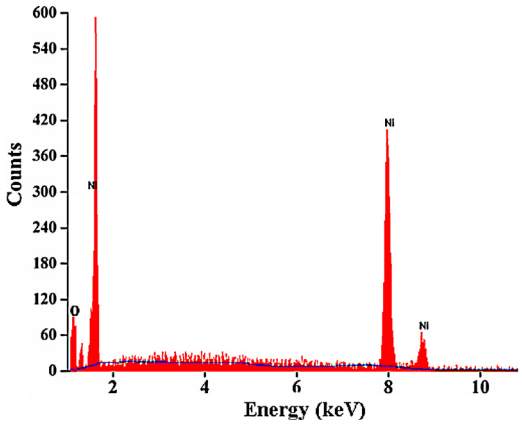


Fig. 6. EDAX spectra of Ni nanoparticles (sample-B).

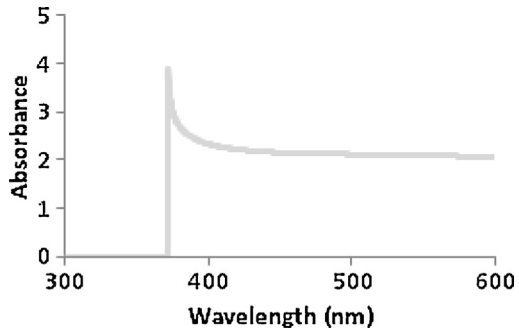


Fig. 7. Optical absorption spectra of nickel nanoparticles (sample-A).

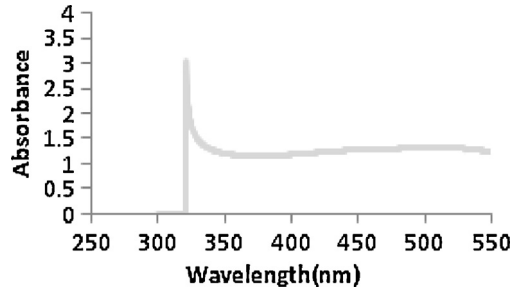


Fig. 8. Optical absorption spectra of nickel nanoparticles (sample-B).

4.46 nm in Ni-2-propanol system shows an absorption band at 212 nm.

According to UV–vis spectroscopy, electrons are transferred from low-energy to high-energy atomic or molecular orbital's when the material is irradiated with light. Such electron transfer processes may take place in transition metal ions like nickel. The position of the absorbance maximum is not fixed but depends partially on the solvent in which the sample may be dissolved and on the molecular environment of the chemical functionalities that are responsible for absorption. So, a strong absorption in the UV region is observed at wavelengths about 371 nm for the particle size of 23.64 nm (sample-A) and 321 nm for the particle size of 18.62 nm (sample-B).

A protective layer from ethylene glycol might form on the particles (samples-A and -B) surface while synthesizing. So the energies of the quantum states of the molecules are somewhat spread out due to constant collisions with the surrounding ethylene glycol molecules. Therefore the samples (A and B) absorb photons spread over a range of wavelength and the spectrum acquires the shape of a smooth and continuous absorption peak. The difference in position of the absorption band in the present investigation may probably due to the effect of excess addition of hydrazine which in turn increases the quantum confinement [25]. It confirms the presence of nickel nanoparticles. Fig. 9 shows optical transmittance spectra of the samples (A and B). The samples are transparent in a large range of wavelength.

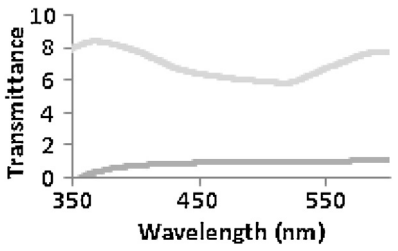


Fig. 9. Optical transmittance spectra of nickel nanoparticles (sample-A and -B).

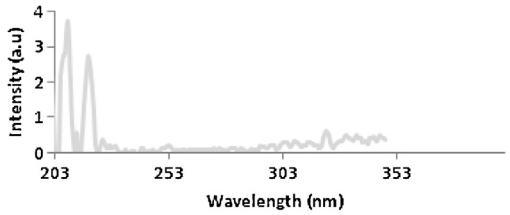


Fig. 10. Photoemission spectrum of nickel nanoparticles (sample-A).

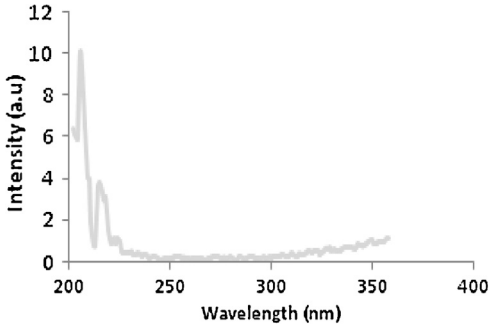


Fig. 11. Photoemission spectrum of nickel nanoparticles (sample-B).

3.5. PL studies

Fig. 10 shows the photoemission characteristics of nickel nanoparticles at 371 nm (sample-A). Two characteristic emission bands are observed at 209 nm and 217 nm with intensities 3.71 and 2.73 respectively. Fig. 11 represents the photoemission characteristics of nickel nanoparticles at 371 nm (sample-B). Two characteristic emission bands are observed at 205 nm and 215 nm with intensities 10.1 and 3.60 respectively. The sharp lines are characteristic of radiative transitions at deep neutral defects in nickel nanoparticles, which are known from other studies involving XRD, EDAX and optical spectra. The PL spectrum correlates well that in these Nickel samples, the impurity state does not appear and the narrow PL lines indicates the good uniformity of nickel nanoparticles and its high quality. The emission peaks found in the PL spectra for sample-A and sample-B are the characteristic features of nickel nanoparticles occurring due to the effect of quantum size confinement. In addition, changes in PL intensity for these nickel samples may be due to the change in concentration and increase in the confinement energy which leads to substantial blue shifts in the PL spectra.

4. Conclusion

Nickel nanoparticles have been synthesized by hydrazine reduction method of nickel chloride in ethylene glycol at 90 °C without soluble polymer as a protective agent. No extra nitrogen gas was required to create an inert atmosphere due to the addition of NaOH trace. The resultant particles have been characterized and found to be pure nickel crystalline of FCC structure by XRD. UV–vis spectroscopy curves were observed to be sensitive to the characteristics of the nanoparticles and the absorption spectra present an absorption edge at 320–371 nm. Photoluminescence characteristics strongly revealed the presence of quantum confinement effect in nickel nanoparticles.

References

[1] I.G. David, B. Donald, J.S. David, J.N. Richard, A nanometre-scale electronic switch consisting of a metal cluster and redox-addressable groups, Nature 408 (2000) 67–69.
[2] L. Lu, L.B. Wang, B.Z. Ding, High-tensile ductility in nano crystalline copper, J. Mater. Res. 15 (2000) 270–273.
[3] C. Petit, T. Cren, D. Roditchev, W. Sacks, J. Klein, M.P. Peleni, Single electron tunneling through nano sized cobalt particles, Adv. Mater. 11 (1999) 1198–1202.
[4] S. Link, Z.L. Wang, How does a gold nanorod melt? J. Phys. Chem. 104B (2000) 7867–7870.
[5] R. Suryanarayanan, C.A. Frey, S.M.L. Sastry, B.E. Waller, S.E. Bates, W.E. Buhro, Mechanical properties of nanocrystalline copper produced by solution phase synthesis, J. Mater. Res. 11 (1996) 439–448.
[6] P. Song, D. Wen, Z.X. Guo, T. Korakianitis, Oxidation investigation of nickel nanoparticles, Phys. Chem. Chem. Phys. 10 (2008) 5057–5065.
[7] D.H. Chen, S.H. Wu, Synthesis of nickel nanoparticles in water-in-oil microemulsions, Chem. Mater. 12 (2000) 1354–1360.
[8] C.Y. Liu, L.H. Lin, New pathway for the synthesis of ultrafine silver nanoparticles from bulk silver substrates in aqueous solutions by sonoelectrochemical methods, Electrochem. Commun. 6 (2004) 1163–1168.
[9] H. Wu, D.H. Chen, Synthesis and characterization of nickel nanoparticles by hydrazine reduction in ethylene glycol, J. Colloid Interface Sci. 259 (2003) 282–286.
[10] Y.L. Hou, S. Gao, Monodisperse nickel nanoparticles prepared from a monosurfactant system and their magnetic properties, J. Mater. Chem. 13 (2003) 1510–1512.
[11] K.S. Chou, C.Y. Ren, Synthesis of nanosized silver particles by chemical reduction method, Mater. Chem. Phys. 64 (2000) 241–246.
[12] P. Christophe, L. Patricia, P. Marie-Paule, In situ synthesis of silver nanocluster in AOT reverse micelles, J. Phys. Chem. 97 (1993) 12974–12983.
[13] G. Sandmann, H. Dietz, W. Plieth, Preparation of silver nanoparticles on ITO surfaces by a double-pulse method, J. Electroanal. Chem. 491 (2000) 78–86.
[14] K. Mallick, M.J. Witcomb, M.S. Scurrell, Self-assembly of silver nanoparticles in a polymer solvent: formation of a nanochain through nanoscale soldering, Mater. Chem. Phys. 90 (2005) 221–224.
[15] Y. Mizukoshi, K. Okitsu, Y. Maeda, T.A. Yamamoto, R. Oshima, Y. Nagata, Sonochemical preparation of bimetallic nanoparticles of gold/palladium in aqueous solution, J. Phys. Chem. B 101 (1997) 7033–7037.
[16] R.S. Ningthoujam, N.S. Gajbhiye, S. Sharma, Reduction mechanism of Ni^{2+} into Ni nanoparticles prepared from different precursors: magnetic studies, Pramana 72 (2009) 577–586.
[17] C.H. Bae, S.H. Nam, S.M. Park, Formation of silver nanoparticles by laser ablation of a silver target in NaCl solution, Appl. Surf. Sci. 197 (2002) 628–634.
[18] X.M. Ni, X.B. Su, Z.P. Yang, H.G. Zheng, The preparation of nickel nanorods in water-in-oil microemulsion, J. Cryst. Growth 252 (2003) 612–617.
[19] A.B. Smetana, K.J. Klabunde, C.M. Sorensen, Synthesis of spherical silver nanoparticles by digestive ripening, stabilization with various agents, and their 3-D and 2-D superlattice formation, J. Colloid Interface Sci. 284 (2005) 521–526.
[20] P.Y. Silvert, K. Tekaia-Elhsissen, Synthesis of monodisperse submicronic gold particles by the polyol process, Solid State Ionics 82 (1995) 53–60.
[21] A.S. Lanje, S.J. Sharma, R.B. Pode, Dielectric study of tin oxide nanoparticles at low temperature, Arch. Appl. Sci. Res. 2 (2010) 127–135.
[22] Y.L. Hou, S. Gao, Solvothermal reduction synthesis and magnetic properties of polymer protected iron and nickel nanocrystals, J. Alloys Compd. 365 (2004) 112–116.
[23] X.F. Yu, X. Liu, K. Zhang, Z.Q. Hu, The lattice contraction of nanometer sized Sn and Bi particles produced by an electrohydrodynamic technique, J. Phys.: Condens. Matter 11 (1999) 937–944.
[24] A. Curtis, D. Duff, P. Edwards, D. Jefferson, B. Johnson, A. Kirkland, A. Wallace, Preparation and structural characterization of an unprotected copper sol, J. Phys. Chem. 92 (1988) 2270–2275.
[25] J.A. Creighton, D.G. Eadon, Ultraviolet–visible absorption spectra of the colloidal metallic elements, J. Chem. Soc. Faraday Trans. 87 (1991) 3881–3891.